

A new Topology of a High-Voltage-Gain DC–DC Converter Based on Modified Greinacher Voltage Multiplier

Mohammad Altimania, Mohamad Saleh Sanjari Nia, Mehdi Ferdowsi, and Pourya Shamsi

Department of Electrical and Computer Engineering

Missouri University of Science and Technology

{mragy9, mswvq, ferdowsi, shamsip}@mst.edu

Abstract—This paper proposes a new topology of a non-isolated two-phase interleaved boost dc–dc converters with modified Greinacher voltage multiplier cells (VMCs) in continuous conduction mode (CCM). The proposed topology can quickly achieve a high gain with low stress on components and proper duty cycle. Moreover, this topology requires a small inductance size in CCM while maintaining the continuity of the input current due to the interleaved technique used in this converter. Because of these features, this topology can be used in many renewable applications such as PV, DC microgrids, etc. The design procedures and component selection are presented in this paper. Furthermore, the proposed converter was simulated to convert an input voltage of 20 V to output voltage of 400 V with an output power of 200 W. Finally, experimental results have been provided to confirm the analysis and simulation results.

Index Terms—High-voltage-gain converter, two-phase interleaved boost converter, modified Greinacher cells, voltage multiplier cells (VMCs), and continuous conduction mode (CCM).

I. INTRODUCTION

IN recent years, in data centers, microgrids, and residential buildings, the DC distribution system of 400V has attracted more attention. Lower cost, higher efficiency, and reliability are the advantages of the 400V distribution DC system [1]. On the other hand, due to the economic and environmental challenges, renewable energy systems, especially solar systems, are becoming more widespread [2]. To increase the output of the photovoltaic, which is between 20V–40V, to 400V, high voltage gain dc–dc converters are necessary. Using traditional power electronics converters such as boost or buck-boost converters lead to lower efficiency and high voltage stress on the components [3]. Moreover, other topologies such as flyback, forward, and half/full-bridge, push-pull converters cannot be useful because those converters need larger input capacitance due to the discontinuous input current [4], [5].

In [6]–[9], different HVG dc–dc converters with voltage multiplier (VM) are discussed. In [6], the proposed topology led to low voltage on the elements, but the large input current ripple is its drawback. Also, in [7], a step-up converter using inductors energy cell-based switch capacitor is proposed. Despite low voltage stress on the components, in many cases described in [8], the voltage gain is not enough to reach 400V. Moreover, in [9], a non-transformer boost converter with continuous input current is proposed. The voltage gain is sufficient to achieve the output of 400V. However, the voltage stress on switches, diodes, and capacitors is high, which leads to lower efficiency and more expensive elements.

Other topologies that are useful for high voltage gain dc–dc

converters are the ones with magnetic parts such as coupled inductors and high-frequency transformers. In [10]–[13], different isolated topologies are discussed and analyzed. However, the converters with magnetic parts show other problems such as voltage spike, leakage inductance, parasitic capacitance, and higher voltage stress on the switches, which require clamp circuits. Using clamp circuits reduce the efficiency and decrease the voltage gain.

In [14]–[16], topologies with interleaved boost using the Cockroft-Walton voltage multiplier were proposed. These topologies provide many advantages such as lower voltage stress, however, as the number of multiplier stages increases the output impedance rapidly increases, and the efficiency and the voltage gain decrease.

This paper proposes a new family of a non-isolated two-phase interleaved boost dc–dc converters with modified Greinacher voltage multiplier cells in CCM. This proposed family can be operated by either a single or dual voltage sources. The voltage multiplier stage in this family is expandable to increase the voltage gain further as well to reduce the voltage stress on the components while maintaining the continuity of input current. As a result, this family can be used in many renewable energy applications, and other applications for those need such features. The rest of the paper is organized as follows, the proposed converter topology is presented, and different modes of operation are discussed in Section II. The voltage gain of the family, current, and voltage stresses of some components are derived in Section III. The simulation and experimental results are presented in Section IV. At last, section V concludes the paper.

II. PROPOSED CONVERTER AND OPERATIONAL PRINCIPLE IN CCM

The proposed converter is shown in Fig. 1, where V_{in1} and V_{in2} are two input voltage sources; S_1 and S_2 are power MOSFET switches; L_1 and L_2 are the power inductors; D_1 to D_6 are power diodes; C_1 to C_6 are capacitors; R is the load resistance. This topology consists of two stages. The first stage is interleaved boost stages with a two-phase, and this stage can be powered by either a single or two input sources. The second stage is the voltage multiplier stage, which is used to increase dc–voltage further and reduces stresses on the components. The first cell on the voltage multiplier stage is Greinacher voltage multiplier that consists of four diodes and four capacitors. The second cell on the voltage multiplier stage consists of two diodes and two capacitors. This topology is inspired by a

Greinacher voltage multiplier [1]–[3].

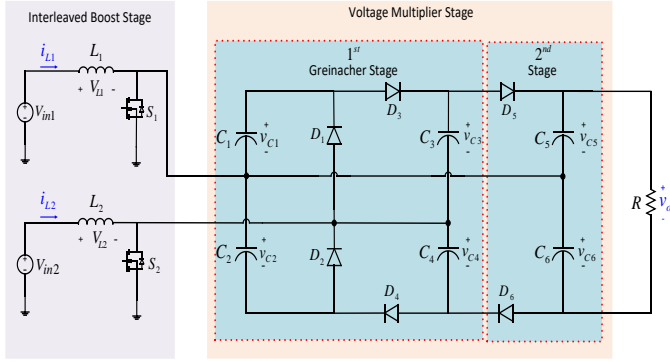


Fig. 1. The proposed converter with a voltage multiplier stage.

Additionally, two switches should not be off at the same time, and the phase shift between the gate signals of the two switches has been chosen in this study to be 180° . Fig. 2 shows the switching signals with a 180° phase shift, where M_1 to M_4 are operating modes, T is the switching period, and d_1 and d_2 are duty ratios of switch one and two, respectively.

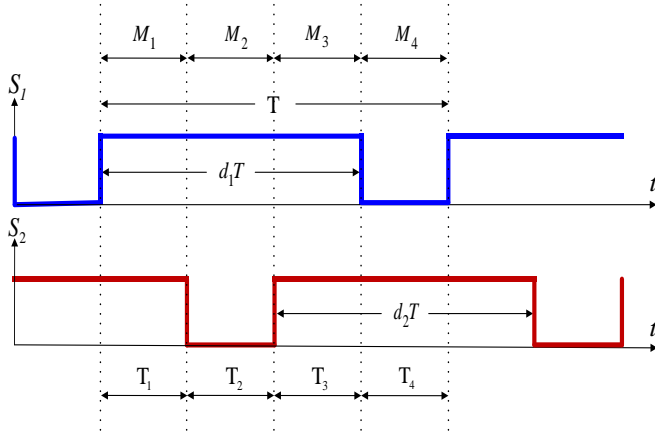


Fig. 2. Waveforms of the switching signals during one switching cycle.

Also, some assumptions are made during the analysis of this topology, such as components are ideal; current of two inductors are in CCM; the topology operates in steady-state; capacitors are very large; parasitic parameters are neglected. During the analysis and investigation of proposed topology in CCM, there are four operating modes at each switching period. For simplicity, these operating modes of the topology with one input source and the two voltage multiplier cells will be presented as follows:

A. Mode 1:

For this operation mode, both power switches S_1 and S_2 of the converter are ON, and this mode ends when S_2 is OFF. Consequently, two inductors are getting energized from the input source and both inductor currents i_{L1} and i_{L2} are linearly increased. Moreover, the voltage across these two inductors is equal to V_{in} . Furthermore, all voltage multiplier diodes are OFF, and all capacitors are disconnected during this mode, as depicted in Fig. 3. Therefore, capacitors C_5 and C_6 are providing energy to the load.

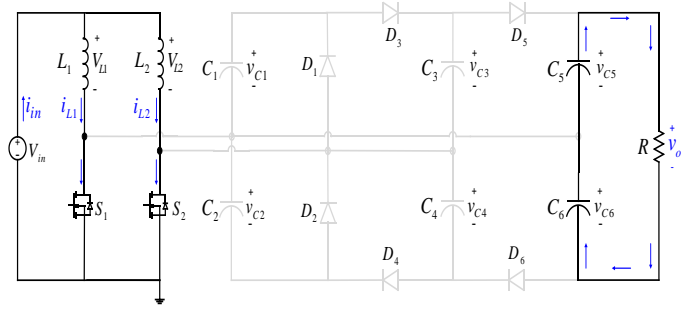


Fig. 3. Equivalent circuit of Mode 1 during one switching cycle.

B. Mode 2:

In this time interval, power switch S_1 is still ON, while S_2 is turned OFF, and this mode finishes when both power switches are ON as in Mode 1. Thus, inductor L_1 is still in charging mode, and the voltage across this inductor is equal to V_{in} . In contrast, inductor L_2 is releasing energy in this mode and the current i_{L2} decreases linearly in this mode. Additionally, diodes D_1 , D_4 , and D_5 are turned ON, whereas diodes D_2 , D_3 , and D_6 are turned OFF, as described in Fig. 4. Accordingly, capacitor C_1 , C_4 , and C_5 are charging, while capacitors C_2 , C_3 , and C_6 are discharging. Therefore, a part of diode $D_{2,1}$ current ($i_{D2,1}$) is supplying energy into the load while the remainder of this current is charging capacitor C_5 .

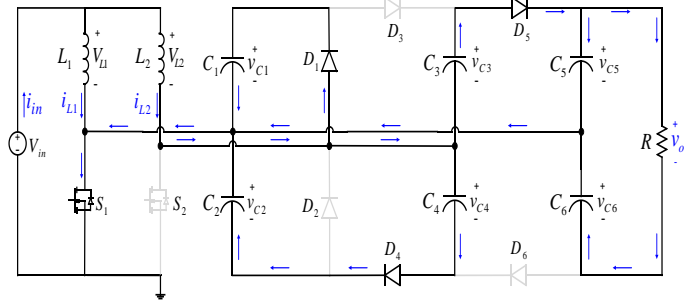


Fig. 4. Equivalent circuit of Mode 2 during one switching cycle.

C. Mode 3:

This mode is the same as Mode 1.

D. Mode 4:

In this period, switch S_1 is turned OFF, while S_2 is still ON and this mode ends when S_1 is turned ON. Subsequently, inductor L_1 is in discharging mode, and i_{L1} decreases linearly. Meanwhile, L_2 is still in the charging mode and i_{L2} increases linearly, and also inductor L_2 voltage is equal to V_{in} as in Mode 1 and 3. Moreover, diodes D_1 , D_4 , and D_5 are reverse-biased (OFF), whereas diodes D_2 , D_3 , and D_6 are forward-biased (ON). Hence, capacitors C_2 , C_3 , and C_6 are charging, while capacitors C_1 , C_4 , and C_5 are discharging, as shown in Fig. 6. Lastly, current coming from capacitor C_5 is providing energy into the load.

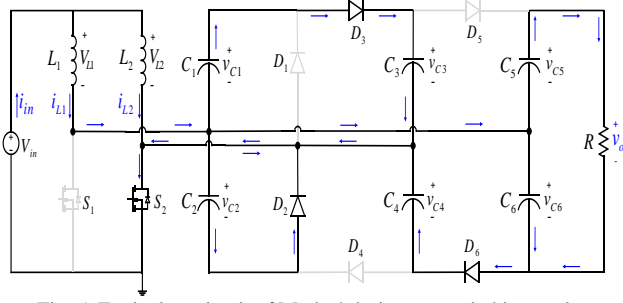


Fig. 5. Equivalent circuit of Mode 4 during one switching cycle.

III. VOLTAGE GAIN AND COMPONENT SELECTION OF THE PROPOSED CONVERTER

After investigating the operating modes of the converter with the two VM cells, the voltage-second balance of both inductors can be used to find the voltage gain ratio for this topology. Thus, the average voltage across inductor L_1 and L_2 is zero for periodic operation

$$\langle v_{L1} \rangle = 0, \text{ and } \langle v_{L2} \rangle = 0 \quad (1)$$

From (1), Kirchhoff's voltage law can be used to find (2) and (3)

$$\begin{aligned} V_{C2} = V_{C3} - V_{C1} = V_o - V_{C4} - V_{C5} = V_{C6} - V_{C4} \\ = \frac{V_{in}}{1 - d_1} \end{aligned} \quad (2)$$

$$\begin{aligned} V_{C1} = V_{C5} - V_{C3} = V_o - V_{C3} - V_{C6} = V_{C4} - V_{C2} \\ = \frac{V_{in}}{1 - d_2} \end{aligned} \quad (3)$$

From (2) and (3), the voltage across each capacitor and output can be found as follow:

$$V_{C1} = \frac{V_{in}}{1 - d_2} \quad (4)$$

$$V_{C2} = \frac{V_{in}}{1 - d_1} \quad (5)$$

$$V_{C3} = V_{C4} = \frac{V_{in}}{1 - d_1} + \frac{V_{in}}{1 - d_2} \quad (6)$$

$$V_{C5} = \frac{V_{in}}{1 - d_1} + \frac{2V_{in}}{1 - d_2} \quad (7)$$

$$V_{C6} = \frac{2V_{in}}{1 - d_1} + \frac{V_{in}}{1 - d_2} \quad (8)$$

$$\frac{V_o}{V_{in}} = \frac{3}{1 - d_1} + \frac{3}{1 - d_2} \quad (9)$$

If both duty cycles are assumed to be equal, then the voltage ratio can be written as follows

$$\frac{V_o}{V_{in}} = \frac{6}{1 - d} \quad (10)$$

For equal duty cycles, Fig. 6 shows the voltage gain versus the duty cycle for this topology. As it can be seen that the voltage

gain for this converter increases as duty cycle increase and it can easily achieve a voltage gain of 20.

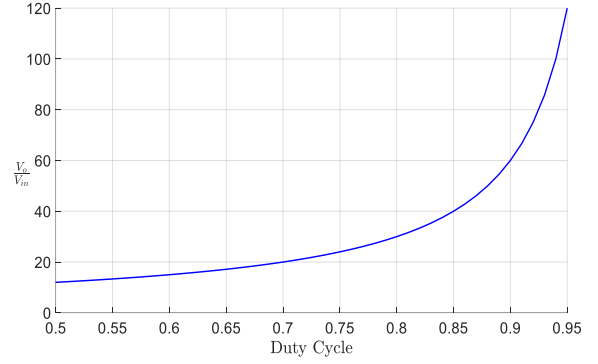


Fig. 6. The voltage gain of topology versus duty cycle in CCM.

The peak blocking voltage of both the switches of topology can be computed by

$$V_{S1} = \frac{V_{in}}{1 - d_2} \quad (11)$$

$$V_{S2} = \frac{V_{in}}{1 - d_1} \quad (12)$$

The maximum blocking voltage across VM diodes are equal to each other, and it can be calculated by

$$V_{Dk} = \frac{V_o}{3} \quad (13)$$

The average, maximum, minimum and RMS values of both inductor currents are given by

$$I_{L1,avg} = \frac{3I_o}{1 - d_1} \quad (14)$$

$$I_{L2,avg} = \frac{3I_o}{1 - d_2} \quad (15)$$

$$I_{L1,max} = \frac{3I_o}{1 - d_1} + \frac{V_{in}d_1}{2L_1f} \quad (16)$$

$$I_{L2,max} = \frac{3I_o}{1 - d_2} + \frac{V_{in}d_2}{2L_2f} \quad (17)$$

$$I_{L1,min} = \frac{3I_o}{1 - d_1} - \frac{V_{in}d_1}{2L_1f} \quad (18)$$

$$I_{L2,min} = \frac{3I_o}{1 - d_2} - \frac{V_{in}d_2}{2L_2f} \quad (19)$$

$$I_{L1,rms} = \sqrt{\left[\frac{3I_o}{1 - d_1}\right]^2 + \left(\frac{V_{in}d_1}{2\sqrt{3}L_1f}\right)^2} \quad (20)$$

$$I_{L2,rms} = \sqrt{\left[\frac{3I_o}{1 - d_2}\right]^2 + \left(\frac{V_{in}d_2}{2\sqrt{3}L_2f}\right)^2} \quad (21)$$

To operate the topology in CCM, the following equations can be used to obtain the minimum inductor size of both inductors

$$L_{1,crit} = \frac{(1 - d_1)d_1V_{in}}{6I_0f} \quad (22)$$

$$L_{2,crit} = \frac{(1 - d_2)d_2V_{in}}{6I_0f} \quad (23)$$

The average diode currents for all diodes are equal to the output current which can be written as

$$I_{D,odd,avg} = I_{D,even,avg} = I_{D,o,avg} = I_o \quad (24)$$

The RMS currents of diodes are

$$I_{D,2,3,6,rms} = \sqrt{\left[\frac{3I_o}{1 - d_1}\right]^2 + \left(\frac{V_{in}d_1}{2\sqrt{3}L_1f}\right)^2} \quad (25)$$

$$I_{D,1,4,5,rms} = \sqrt{\left[\frac{3I_o}{1 - d_2}\right]^2 + \left(\frac{V_{in}d_2}{2\sqrt{3}L_2f}\right)^2} \quad (26)$$

IV. SIMULATION AND EXPERIMENTAL RESULTS

PLECS with MATLAB was used to confirm the operating principle of this topology in CCM. To accomplish 214 W at 413.8 V output voltage, the following parameters have been selected such as a 20 V for the input voltage, 150 kHz for the switching frequency, 71% for the duty cycle, 15 μ H for both inductors, and 800 Ω for the load, and Table I lists the selected parameters used in the simulation. Moreover, some resistances have been added with some components during the simulation. The output voltage and power after running the simulation are 406 V and 206 W, respectively, and the major waveforms are shown in Figs. 7–11. The waveforms of the two switching signals, output voltage, output current, and input current are depicted in Fig. 7. The voltage across each inductor and each active switch are given in Fig. 8. The absolute blocking voltage across switch 1 and switch 2 is only 68.89 V, which is approximately equal to one-sixth of the output voltage. 8.39 A, 5.25 A, and 5.55 A are the peak, mean, and RMS values of each inductor currents from the simulations. Also, the maximum, mean, and RMS values of each switch current are 12.35 A, 5.25 A, and 6.78 A, respectively. The current waveforms of two inductors and two switches are shown in Fig. 9. Additionally, the absolute maximum voltage across each diode is only 136.27 V, which is almost equal to one-third of the output voltage, and the voltage waveforms across all diodes are depicted in Fig. 10. Moreover, the voltage waveforms across each capacitance are given in Fig. 11. The average voltage across capacitors 1 and 2 is 67.74 V; the average voltage across capacitors 3 and 4 is 135.36 V, and the average voltage across capacitors 3 and 4 is 203 V.

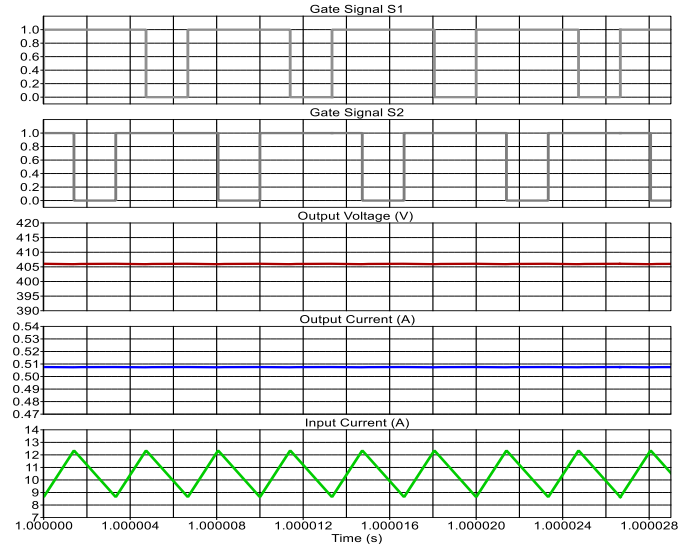


Fig. 7. Simulation waveforms: The two switching signals, output voltage, output current, and input current.

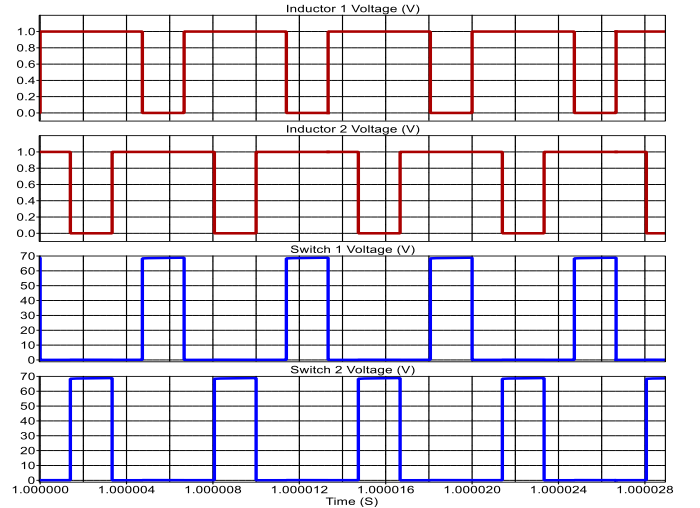


Fig. 8. Simulation waveforms: Voltage of two inductors and two active switches.

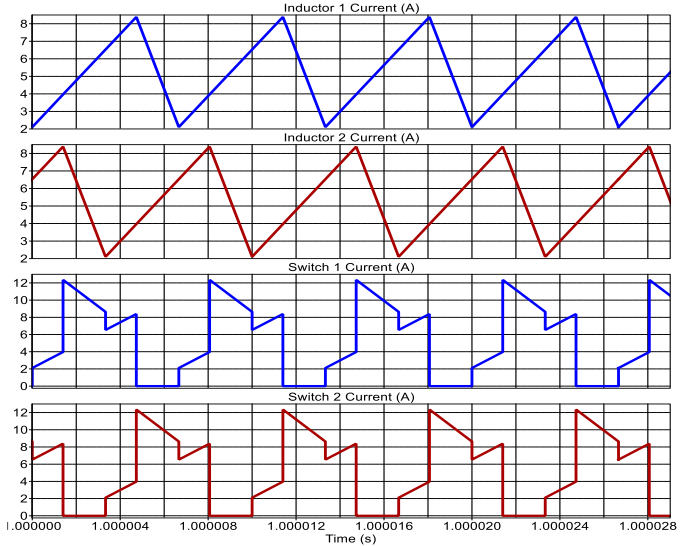


Fig. 9. Simulation waveforms: Current of two inductors and two active switches.

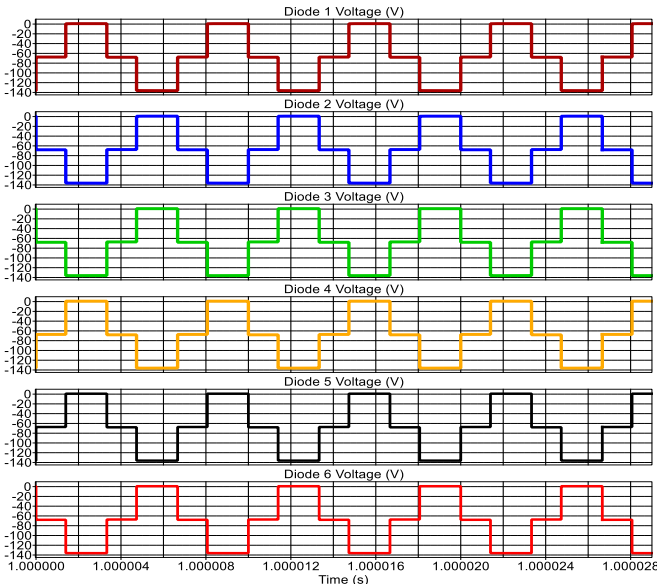


Fig. 10. Simulation waveforms: Voltages of all diodes.

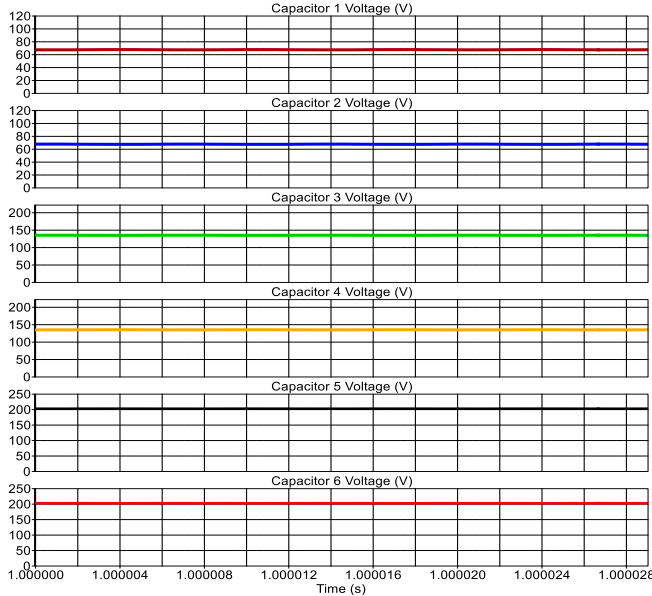


Fig. 11. Simulation waveforms: Voltages of all capacitors.

TABLE I
COMPONENTS LIST

Component	Value
Input voltage	20 V
Frequency	150 kHz
Duty Ratio	0.71
Load	800 Ω
Inductors: L_1 and L_2	15 μH
Capacitors: C_1 to C_7	10 μF

For experimental results, Table II summarizes the selected components used for implementing a hardware prototype and Fig. 12 shows the hardware prototype used in the experiment. A 20 V from a dc power supply was used as the input source for the converter, and 800 Ω of a mix of load resistors was used

as the load. Some waveforms resulting from the experiment are given in Figs. 13–15 and they agree both the calculations and simulation results.

TABLE II
COMPONENTS LIST

Item	Designation	Rating	Part No.
MOSFETs	S_1 and S_2	$V_{ds} = 150 \text{ V}$ $R_{on} = 2.7 \text{ m}\Omega$	IRF150P220
Inductors	L_1 and L_2	$L = 15 \mu\text{H}$ $R_L = 1.441 \text{ m}\Omega$	74436411500
Diodes	D_1 to D_4	$V_r = 250 \text{ V}$ $I_F = 40 \text{ A}$ $V_F = 0.86 \text{ V}$	MBR40250G
Capacitors	C_1 to C_4	10 μF	MKP1848C61050JK2

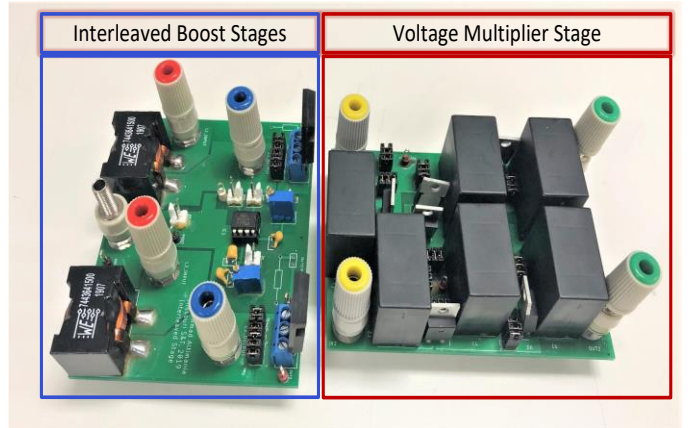


Fig. 12. The hardware prototype.

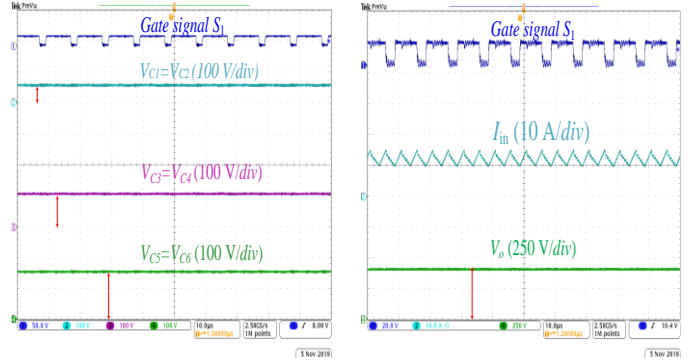


Fig. 13. Experimental waveforms: Voltage stresses across capacitors, input current, and output voltage.

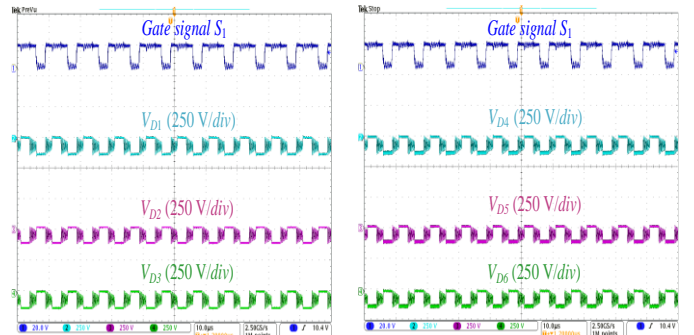


Fig. 14. Experimental waveforms: Voltage stresses across diodes

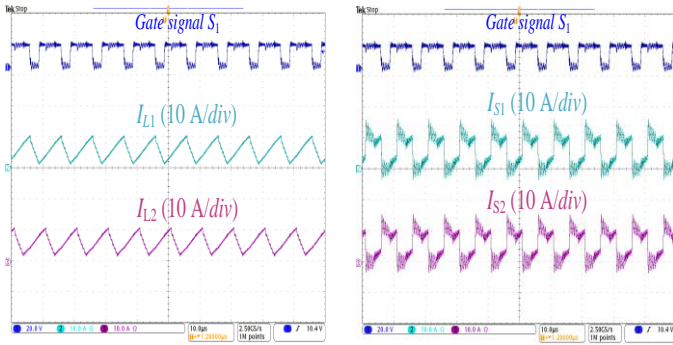


Fig. 15. Experimental waveforms: Current of two inductors and two MOSFETs.

V. CONCLUSION

In this paper, a new topology of a non-isolated high-voltage-gain dc-dc converter based on modified Greinacher voltage multiplier is presented. The proposed topology can be operated by either a single or two input voltage sources. In this paper, the voltage gain equation and other essential equations required for components selection of the topology is illustrated thoroughly. In addition, the theoretical analysis of the converter was confirmed by the simulation and experimental results. The proposed converter can achieve a high gain while having low stress on components. Moreover, this converter has continuous input current that will make this topology a preferable choice for renewable energy applications. Accordingly, the proposed topology can be used in many applications that have low-voltage sources and required a high gain such as PV, automobile headlight (HID), fuel cell, etc.

REFERENCES

- [1] A. Alzahrani, P. Shamsi, and M. Ferdowsi, "A novel interleaved non-isolated high-gain DC-DC boost converter with Greinacher voltage multiplier cells," *2017 IEEE 6th International Conference on Renewable Energy Research and Applications (ICRERA)*, San Diego, CA, 2017, pp. 222-227.
- [2] M. Altimania, A. Alzahrani, M. Ferdowsi and P. Shamsi, "Operation and Analysis of Non-Isolated High-Voltage-Gain DC-DC Boost Converter with Voltage Multiplier in the DCM," *2019 IEEE Power and Energy Conference at Illinois (PECI)*, Champaign, IL, USA, 2019, pp. 1-6.
- [3] M. Forouzesh, Y. P. Siwakoti, S. A. Gorji, F. Blaabjerg, and B. Lehman, "Step-Up DC-DC Converters: A Comprehensive Review of Voltage-Boosting Techniques, Topologies, and Applications," in *IEEE Transactions on Power Electronics*, vol. 32, no. 12, pp. 9143-9178, Dec. 2017.
- [4] B. P. R. Baddipadiga, V. A. K. Prabhala and M. Ferdowsi, "A Family of High-Voltage-Gain DC-DC Converters Based on a Generalized Structure," in *IEEE Transactions on Power Electronics*, vol. 33, no. 10, pp. 8399-8411, Oct. 2018.
- [5] M. Altimania, M.S. Sanjarinia, M. Ferdowsi, and P. Shamsi, "Analysis and Modeling of a Non-Isolated Two-Phase Interleaved Boost Converter with Diode-Capacitor Cells in the DCM," *2019 North American Power Symposium (NAPS)*, 2019.
- [6] B. Wu, S. Li, Y. Liu, and K. M. Smedley, "A New Hybrid Boosting Converter for Renewable Energy Applications," *IEEE Transactions on Power Electronics*, vol. 31, no. 2, pp. 1203-1215, 2016.
- [7] G. Wu, X. Ruan, and Z. Ye, "Nonisolated High Step-Up DC-DC Converters Adopting Switched-Capacitor Cell," *IEEE Transactions on Industrial Electronics*, vol. 62, no. 1, pp. 383-393, 2015.
- [8] Y. Tang, T. Wang, and Y. He, "A Switched-Capacitor-Based Active-Network Converter With High Voltage Gain," *IEEE Transactions on Power Electronics*, vol. 29, no. 6, pp. 2959-2968, 2014.
- [9] J. C. Rosas-Caro, F. Mancilla-David, J. C. Mayo-Maldonado, J. M. Gonzalez-Lopez, H. L. Torres-Espinosa, and J. E. Valdez-Resendiz,

- "A Transformer-less High-Gain Boost Converter With Input Current Ripple Cancellation at a Selectable Duty Cycle," *IEEE Transactions on Industrial Electronics*, vol. 60, no. 10, pp. 4492-4499, 2013.
- [10] S. Li, E. Rong, Q. Min, and S. Lu, "A Half-Turn Transformer With Symmetry Magnetic Flux for High-Frequency-Isolated DC/DC Converters," *IEEE Transactions on Power Electronics*, vol. 33, no. 8, pp. 6467-6470, 2018.
- [11] Y. Yanagisawa, Y. Miura, H. Handa, T. Ueda, and T. Ise, "Characteristics of Isolated DC-DC Converter With Class Phi-2 Inverter Under Various Load Conditions," *IEEE Transactions on Power Electronics*, vol. 34, no. 11, pp. 10887-10897, 2019.
- [12] L. Chen, L. Tarisciotti, A. Costabeber, P. Wheeler, and P. Zanchetta, "Model Predictive Control for Isolated DC/DC Power Converters with Transformer Peak Current Shaving," *2018 IEEE Energy Conversion Congress and Exposition (ECCE)*, 2018.
- [13] M. S. Sanjari Nia, P. Shamsi and M. Ferdowsi, "Investigation of Various Transformer Topologies for HF Isolation Applications," in *IEEE Transactions on Plasma Science*, vol. 48, no. 2, pp. 512-521, Feb. 2020.
- [14] B. Axelrod and Y. Berkovich, "Cockroft-Walton voltage multiplier combined with switched-coupled-inductor boost converter," *2016 IEEE International Energy Conference (ENERGYCON)*, 2016.
- [15] M. S. Bhaskar, S. Padmanaban, F. Blaabjerg, L. E. Norum, and A. H. Ertas, "4Nx Non-Isolated and Non-Inverting hybrid Interleaved Multilevel Boost Converter based on VLSIm Cell and Cockroft Walton voltage multiplier for renewable energy applications," *2016 IEEE International Conference on Power Electronics, Drives and Energy Systems (PEDES)*, 2016.
- [16] B. Axelrod, Y. Berkovich, and Y. Beck, "High step-up DC-DC converter based on the switched-coupled-inductor boost converter and diode-capacitor multiplier: steady state and dynamics," *IET Power Electronics*, vol. 8, no. 8, pp. 1420-1428, Jan. 2015.